The IR Photochemistry of Organic Compounds. IV.[1] The Infrared Multiple-Photon Decomposition of Cyclic Ethers Induced by a TEA CO_2 Laser

Tetsuro MAJIMA,* Tadahiro ISHII†, and Shigeyoshi ARAI††
The Institute of Physical and Chemical Research (RIKEN),
Hirosawa, Wako, Saitama 351-01
†Science University of Tokyo, Kagurazaka, Shinjuku-ku, Tokyo 162
††Kyoto Institute of Technology, Matsugasaki, Sakyo-ku, Kyoto 606
(Received July 7, 1989)

The mechanism of the infrared multiple-photon decomposition (IRMPD) of saturated cyclic ethers (**1**—**7**) has been systematically studied on the basis of product analysis, particularly with the aim of finding a suitable cyclic ether for oxygen-isotope separation. The main products are H_2CO, CO, H_2, and lower hydrocarbons. Acetaldehyde is additionally formed in the IRMPD of **1** and **3**—**6**, while acetone is produced only in the IRMPD of **3b**. The initial process is the homolytic cleavage of the C–O bond to yield the corresponding biradical with a high internal energy. The biradical decomposes sequentially of through secondary IRMPD to yield the primary products with high internal energies. The decomposition of the biradicals proceeds mainly via β-fission, but also partly via γ-fission. Some of the primary products further decompose sequentially or through secondary IRMPD into stable products. Several radical intermediates are trapped with Br_2. The product distributions are clearly dependent on the irradiation parameters. This dependence and the branching ratio are discussed in terms of sequential decomposition, the collisional effect, and the internal energy of the transient species. On the basis of the experimental results, it is suggested that, among cyclic ethers, the best starting ether in the oxygen-isotope separation by a TEA CO_2 laser is tetrahydropyran (**4**).

In the previous paper we have described the infrared multiple-photon decomposition (IRMPD) of saturated open-chain ethers (ROR′; R= R′= alkyl) induced by TEA CO_2-laser irradiation.[2] The initial process is the homolytic cleavage of the C–O bond to yield the corresponding alkyl and alkoxyl radicals with high internal energies. Therefore, the radicals decompose sequentially or through secondary IRMPD within a laser pulse to yield the primary products with high internal energies. Then the primary products also decompose, at least partly either sequentially or through secondary IRMPD, into the stable products. The oxygen atom of the decomposing ether appears mainly in carbon monoxide (CO) as a stable oxygen-containing prodcut after the sequential decomposition of formaldehyde, acetaldehyde, and acetone.

When the ^{18}O selective IRMPD of ethers occurs at the wavenumber resonant to the absorption of the C–^{18}O bond, the selectivity of the cleavage of the C–^{18}O bond is expected to reflect the ^{18}O content in the final product, CO. In fact, the ^{18}O selective IRMPD of dimethyl ether has been successfully performed by Vizhin et al.,[3] by Kutschke et al.,[4] and the present authors.[5] On the other hand, no study of oxygen-isotope separation in the IRMPD of cyclic ethers has been reported. The mechanistic studies of the IRMPD of 2,5-dihydrofuran,[6] tetrahydrofuran,[7] methylated tetrahydrofuran,[8] oxetanes,[9] and tetramethyldioxetane[10] show that the cleavage of the C–O bond is involved in the initial step. Therefore, the ^{18}O selective IRMPD can be expected to occur in some cyclic ethers.

In the present work we have systematically studied the mechanism of the IRMPD of saturated cyclic ethers, oxacycloalkanes containing two to six methylene groups and one or two oxygen atoms (**1**—**7**), in order to find a suitable cyclic ether for oxygen-isotope separation. We have analyzed the stable decomposition products. Several intermediates have been trapped by Br_2 in the presence of Br_2. The effects of the irradiation parameters have been studied with respect to a branching ratio of competitive pathways in the decomposition of the transient species. On the basis of the results, it is discussed whether or not cyclic ether is suitable for use as a starting material and which is the best such starting material.

Experimental

The experimental procedure has been described in the previous work.[2] Briefly, the beam from a TEA CO_2 laser was passed through a 1-cm aperture and focused, by means of BaF_2 lens with focal length of 7.5 or 20 cm, into the center of a Pyrex reaction cell. The cells were cylindrical Pyrex tubes 10 and 36 cm long and with volumes of 50 and 132 cm^3 respectively. The incident laser power was attenuated using polyethylene films and was measured with a disk calorimeter. The laser fluence at the focus was estimated from a focus area of 7.1×10^{-4} or 5×10^{-3} cm^2 for the 7.5- and 20-cm focal-length BaF_2 lenses respectively. After irradiation the samples were analyzed by using an IR spectrometer, a gas chromatograph, and a gas chromatograph-mass spectrometer.

The propylene oxide (**1**), oxetane (**2**), tetrahydrofuran (**3a**), *cis*- and *trans*-2,5-dimethyltetrahydrofuran (**3b**), tetrahydropyran (**4**), oxepane (**5**), 1,3-dioxacyclopentane (**6**), and 1,4-dioxacyclohexane (**7**) were obtained from Tokyo Kasei Kogyo or Nakarai Chemicals. Each ether was distilled and degassed by several freeze (−196 °C)-pump-thaw cycles.

Table 1. Irradiation Parameters in the IRMPD of **1**—**7**[a)]

Ether	λ/cm^{-1}	$10^3\ \varepsilon$/Torr^{-1} cm^{-1}	E_p/J pulse^{-1}	F/J cm^{-2}
1	944.19	0.687	0.270	380
2	982.10	1.26	0.247	348
3a	1078.59	4.87	0.201	283
3b	944.19	1.21	0.218	307
4	1046.85	3.10	0.337	475
5	1078.59	1.24	0.238	335
6	1046.85	2.24	0.327	460
7	944.19	6.26	0.301	424

a) λ, wavenumber of the laser; ε, 1←0 absorption coefficient; E_p, incident pulse energy; F, laser fluence at the focus.

Table 2. Product Yields in the IRMPD of **1**—**7**[a)]

Ether	$10^3 Y_d$/Torr pulse^{-1}	$10^3 Y$/Torr pulse^{-1}			MB/%
		H_2	*O*-compnd	Hydrocarbon	
1	0.37	0.27	0.30	0.35	82
2	1.14	0.11	0.68	0.72	60
3a	1.77	0.52	1.28	1.34	72
3b	1.02	0.31	0.67	0.87	66
4	2.07	1.03	1.35	2.15	65
5	1.61	0.67	1.01	2.23	63
6	1.26	0.46	2.16	0.89	86
7	1.52	0.59	2.25	0.79	74

a) Y_d(Decomposition yield of ether)=[decomposed ether]/(number of pulses), Y (yield of product)=[product]/(number of pulses), and MB (material balance)=[(total pressure of the oxygen-containing products)/{(consumed ether)×(number of oxygen atoms in the ether)}]×100.

Results

Decomposition Yields. The significant IRMPD occurred upon the irradiation of 3-Torr (1 Torr=133.322 Pa) ethers (**1**—**7**) with a focused laser beam at a 283—475 J cm^{-2} focused fluence from a TEA CO_2 laser. The laser line was tuned to the frequency which corresponded to the absorption peak of each ether in the tunable range of the laser. The 1←0 absorption coefficient (ε) at the laser wavenumber (λ) is shown in Table 1. The value of ε changes in the range of 6.9×10^{-4}—6.3×10^{-3} Torr^{-1} cm^{-1}. The incident pulse energy (E_p) and the laser fluence at the focus (F) are also shown in Table 1. When the numbers of the laser pulses were 100—500, the conversions were 10—20%. The decomposition yield (Y_d=[decomposed ether])/(number of pulses)) was found to be 3.0×10^{-4}—2.0×10^{-3} Torr pulse^{-1} (Table 2).

Ethylene oxide (*cyclo*-C_2H_4O) is the smallest cyclic ether, and **1** is the methyl derivative of *cyclo*-C_2H_4O. In contrast to **1**, *cyclo*-C_2H_4O has no strong IR absorption in the tunable range of the laser. We could not detect any decomposition, even if 3 Torr of *cyclo*-C_2H_4O was irradiated with 1000 focused laser pulses (0.2 J pulse^{-1}, 282 J cm^{-2}) at either 934.90 or 1050.40 cm^{-1}. It should be noted that, among the cyclic ethers examined, ε is the smallest and that Y_d is also the smallest in the IRMPD of **1**. Although ε is not clearly correlated with Y_d, the compound with a larger ε value tends to give a larger Y_d value. Therefore, the 1←0 absorption is important for the IRMP excitation of the ether. In addition to the 1←0 absorption, the dissociation energies of the bonds in the initial and sequential processes seriously affect the Y_d in the IRMPD.

Table 3. Relative Yields of the Oxygen-Containing Products

Product	Relative yields of product/%							
	1	**2**	**3a**	**3b**	**4**	**5**	**6**	**7**
CO	84	14	57	56	87	61	13	28
H_2CO	12	86	11	4	6	32	85	72
CH_3CHO	3	0	32	30	7	7	2	0
CH_3COCH_3	0	0	0	10	0	0	0	0

Products. The products were H_2, oxygen-containing compounds (*O*-compnds.), and lower hydrocarbons, whose yields (Y=[product]/(number of pulses)) are shown in Table 2. The yield of an oxygen-containing product relative to the total yield of the oxygen-containing products and the yield of a hydrocarbon product relative to the total yield of the hydrocarbon products are shown for each ether in Tables 3 and 4 respectively. No other products were detected in the IR-spectroscopic, gas-chromatographic, and mass-spectrometric analyses. The material balances were satisfactory, i.e., >60%, as is shown in Table 2, where the material balances (MB) based on the oxygen atoms were calculated thus: MB= [(total pressure of the oxygen-containing products)/{(consum-

Table 4. Relative Yields of Hydrocarbon Products

Product	Relative yields of product/%							
	1	**2**	**3a**	**3b**	**4**	**5**	**6**	**7**
CH_4	25	0	11	3	24	2	63	9
C_2H_6	45	0	1	4	0.8	3	0.5	2
C_2H_4	11	83	61	25	42	7	22	75
C_2H_2	8	17	3	3	16	28	14	14
C_3H_8	7	0	0.5	0.7	1	1	0	0
C_3H_6	0.8	0	20	62	3	0	0	0
cyclo-C_3H_6	0	0	0.7	0	0	0.7	0	0
CH_3CCH	0.8	0	0	0	0	1	0	0
CH_2CCH_2	0.3	0	0	0	2	3	0	0
n-C_4H_{10}	1	0	0	0	0	14	0	0
Δ^1-C_4H_8	0.5	0	2	1	5	8	0	0
i-C_4H_8	0	0	0	0	0	0.4	0	0
$\Delta^{1,3}$-C_4H_6	0	0	0	0	4	2	0	0
Δ^1-C_5H_{10}	0	0	0	0	0.5	22	0	0

ed ether)×(number of oxygen atoms in the ether)}] ×100%.

As the oxygen-containing products, CO and formaldehyde (H_2CO) were obtained in the IRMPD of all ethers (Table 3). Acetaldehyde (CH_3CHO) was also formed in the IRMPD of **1** and **3**—**6**. Acetone (CH_3COCH_3) was obtained in a relative yield of 10% only in the IRMPD of **3b**. Because of the good material balance, the oxygen atoms in the decomposing ether seem mostly to be contained in CO, H_2CO, and CH_3CHO.

The small hydrocarbon products, together with their yields relative to the total yield, are shown in Table 4. The distribution of hydrocarbons shows a correspondence to the structure of the ether. The main hydrocarbon products were such C_2 hydrocarbons as ethane (C_2H_6), ethylene (C_2H_4), and acetylene (C_2H_2). In the IRMPD of **3**, propylene (C_3H_6) was also one of the main products. Considerable amounts of C_4 and C_5 hydrocarbons were formed in the IRMPD of **4** and **5**. It is noteworthy that the product distribution is relatively simple in the IRMPD of **2**, **6**, and **7**. Specifically, only C_2H_4 and C_2H_2 were obtained as the hydrocarbon products in the IRMPD of **2**.

The irradiation of each final product (1.0 Torr) under the same conditions did not cause any IRMPD at all or produced decomposition products in only in a negligibly small yield. Therefore, the final products are stable against laser irradiation.

Trapping of Radical Intermediates by Br_2. In order to confirm the radical species formed primarily, ethers (3.0 Torr) were irradiated in the presence of excess Br_2 (3.0 Torr). It was found that Br_2 can be used as a trapping reagent of the radical species formed initially in the IRMPD of organic compounds. For example, CH_3 and CF_3 radicals were trapped as CH_3Br and CF_3Br in the IRMPD of dimethyl ether–Br_2 and perfluorodimethyl ether–Br_2 mixtures in the studies by Vizhin et al.[3] and by the present authors,[2] respectively. A number of bromine-containing hydrocarbons were detected, while the yields of the products decreased slightly. In the IRMPD of the **1**–Br_2 mixture, methyl bromide (CH_3Br), dibromomethane (CH_2Br_2), ethyl bromide (C_2H_5Br), 1,2-dibromoethane ($C_2H_4Br_2$), and vinyl bromide (CH_2CHBr) were obtained in the ratio of 39:27:12:11:11. This is consistent with the intermediaries of CH_3, CH_2, C_2H_5, CH_3CH, and CH_2CH respectively.

The bromine-containing compounds in the IRMPD of the **4**–Br_2 mixture were mainly C_2H_5Br, C_2H_3Br, and $C_2H_4Br_2$. In addition, C_1 and C_4 bromine-containing compounds, such as CH_3Br, CH_2Br_2, C_4H_9Br, C_4H_7Br, and $C_4H_8Br_2$, were also obtained as minor products. Small amounts of C_3 bromine-containing compounds, such as C_3H_7Br, C_3H_5Br, and $C_3H_6Br_2$, were detected. The ratio among C_1, C_2, C_3, and C_4 bromine-containing products was roughly 9:78:2:11. Therefore, it may be suggeted that C_2H_5, C_2H_3, and C_2H_4 are formed as the main intermediaries, while CH_3, CH_2, C_4H_9, C_4H_7, and C_4H_8 are also produced as the minor intermediaries, together with C_3H_7, C_3H_5, and C_3H_6.

In the IRMPD of the **5**–Br_2 mixture, CH_3Br, C_2H_5Br, CH_2CHBr, C_3H_7Br, C_3H_5Br, $C_5H_{11}Br$, and C_5H_9Br were formed. This is consistent with the intermediaries of such transient species as CH_3, C_2H_5, CH_2CH, C_3C_7, C_3H_5, C_4H_9, C_4H_7, C_5H_{11}, and C_5H_9 respectively. Similarly, the bromine-containing compounds were obtained in the IRMPD of other cyclic ether–Br_2 mixtures. Therefore, a relatively large number of radical intermediates are involved in the IRMPD. In addition, radical–radical reactions well known in pyrolyses at high temperatures contribute to the formation of hydrocarbons, at least in part.

Effects of Irradiation Parameters. The analyses of the final products in the IRMPD of **4** under various conditions of laser irradiation were carried out in order to examine the effects of irradiation parameters on the IRMPD, particularly the branching ratio of the

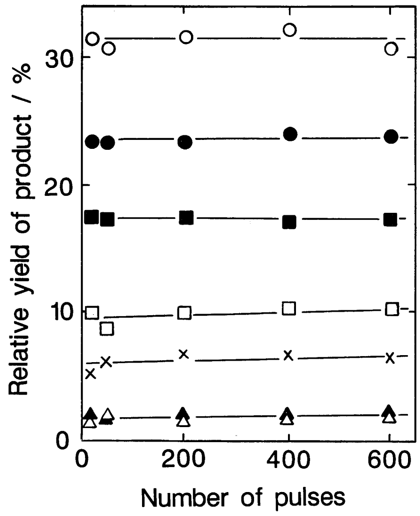

Fig. 1. Effects of number of pulses on relative yields of a product to total yield of all products. H_2 (○), CO (●), H_2CO (△), CH_3CHO (▲), CH_4 (□), C_2H_4 (■), and C_2H_2 (×). P_0, 3.0 Torr; pulse energy, 0.2 J pulse^{-1}; F, 282 J cm^{-2}.

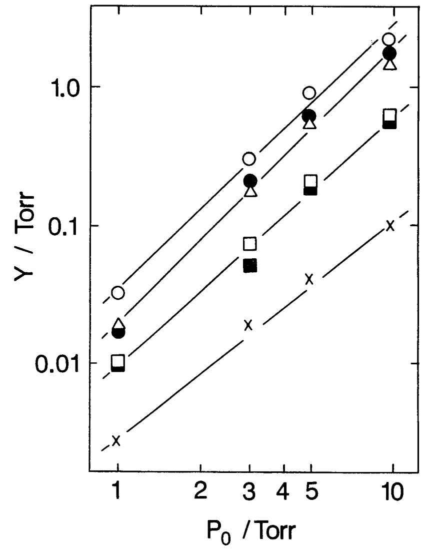

Fig. 2. Plots of product yield (Y) vs. P_0. H_2 (○), C_2H_4 (●), CO (△), CH_4 (□), C_2H_2 (■), and C_3H_6 (×). Number of pulses, 200; pulse energy, 0.2 J pulse^{-1}; F, 282 J cm^{-2}.

competitive pathways.

Number of Laser Pulses: When 3.0 Torr of **4** was irradiated with the CO_2 laser radiation at a pulse energy of 0.2 J and a focus fluence of 282 J cm^{-2}, the consumption of **4** was followed by IR spectroscopy and gas chromatography as a function of the number of laser pulses. Plots of $\ln(P_0/P)$ vs. the number of pulses less than 400 gave a straight line. P_0 and P denote the pressure of **4** before and after irradiation respectively. According to the first-order kinetics, the fractional yield of the decomposition (k_d) is determined to be k_d=8.5×10^{-4} pulse^{-1} from the slope of the straight line.

The yields of the main products increased linearly with the increase in the number of pulses from 20 to 400. The conversion amounted to 27% at 400 pulses. The product distribution did not change with the variation in the number of pulses, as is shown in Fig. 1.

Pressure of 4: The pressure dependence of the product yields for **4** was studied in the range of 0.1—10 Torr. When irradiations of **4** with 200 pulses were carried out at several pressures, the conversions were less than 15%. No dielectric breakdown was observed below 10 Torr. log-log plots of P_0 vs. the product yield (Y) in Torr are shown in Fig. 2. With an increase in P_0, Y increased according to the relation of $Y \propto (P_0)^2$. A log-log plot of P_0 vs. the consumption of **4** ($C=P_0-P$ in Torr) also gave a linear line and the relationship of $C \propto (P_0)^2$.

As is shown in Fig. 3, there were two different pressure regions, below and over 4 Torr. The distribution of the hydrocarbon products was almost independent of the P_0 value over 4 Torr. In contrast, the distribution changed significantly with P_0 below 4 Torr. With an increase in the P_0 value up to 4 Torr, the relative yields of C_2 hydrocarbonds, such as C_2H_4 and C_2H_2, increased considerably, while those of C_3 hydrocarbons, such as C_3H_6 and C_3H_8, decreased sharply. Among the C_4 hydrocarbons, the relative yield of $\Delta^{1,3}$-C_4H_6 increased, while that of Δ^1-C_4H_8 decreased, though only a little. The relative yield of the total C_4 hydrocarbons increased slightly.

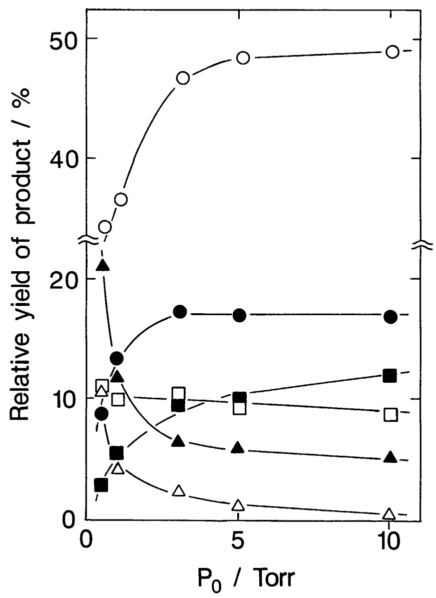

Fig. 3. Effects of P_0 on yields of a hydrocarbon product relative to total yield of all hydrocarbon products. C_2H_4 (○), C_2H_2 (●), C_3H_8 (△), C_3H_6 (▲), Δ^1-C_4H_8 (□), and $\Delta^{1,3}$-C_4H_6 (■). For experimental conditions see the caption in Fig. 2.

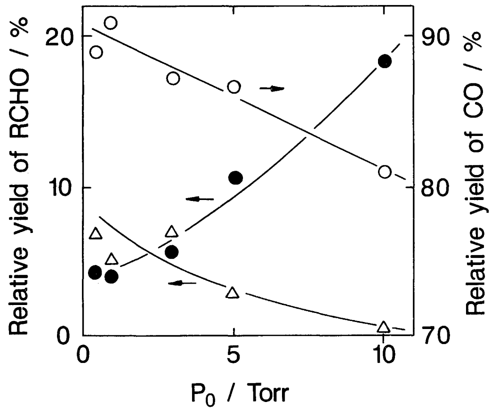

Fig. 4. Effects of P_0 on yield of an oxygen-containing products relative to total yield of all oxygen-containing products. CO (○), H_2CO (●), and CH_3CHO (△). For experimental conditions see the caption in Fig. 2.

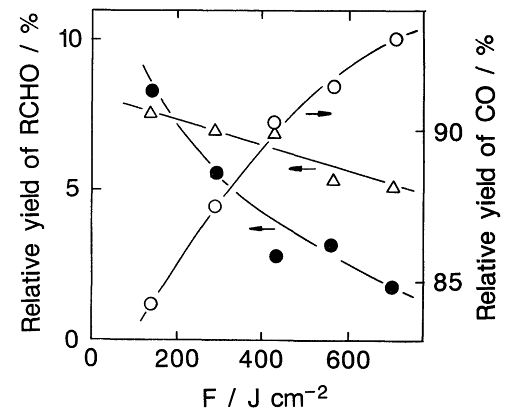

Fig. 6. Effects of F on relative yields of oxygen-containing products. CO (○), H_2CO (●), and CH_3CHO (△). For experimental conditions see the caption in Fig. 5.

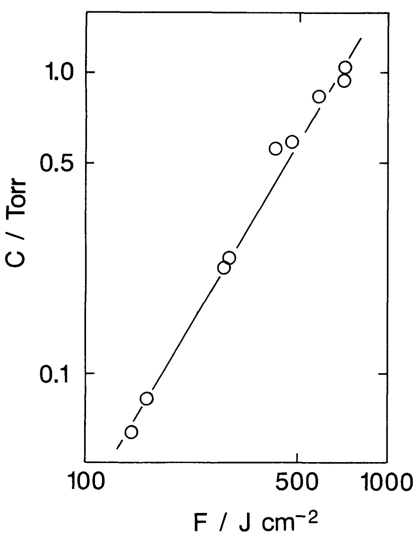

Fig. 5. Plots of conversion (C) vs. laser fluence at the focus (F). Pressure of **4**, 3.0 Torr; number of pulses, 200.

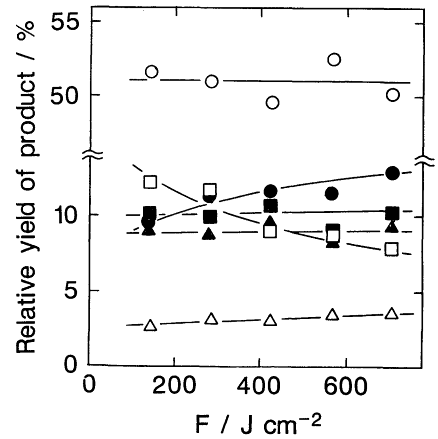

Fig. 7. Effects of F on relative yields of hydrocarbon products. C_2H_4 (○), C_2H_2 (●), C_3H_8 (△), C_3H_6 (▲), Δ^1-C_4H_8 (□), and $\Delta^{1,3}$-C_4H_6 (■). For experimental conditions see the caption in Fig. 5.

The relative yields of oxygen-containing products to the total yield of all oxygen-containing products are plotted against P_0 in Fig. 4. With an increase in P_0, CO and CH_3CHO decreased in their relative yields, while that of H_2CO increased. The material balance based on the oxygen atom falls in the 85—95% range, independently of the P_0 value.

Laser Fluence and Focal Length of Lens: The decomposition yields and product distributions for 3.0 Torr of **4** were examined at various focus fluences (F) using lenses with 7.5- and 20-cm focal lengths. Both the decomposition yield and the total product yield increased with the increase in F in 140—704 J cm^{-2}. The log-log plot of C vs. F in J cm^{-2} showed a relation of $C \propto F^{1.7}$, as is presented in Fig. 5. The total product yield increased with the increase in F. With the increase in F, the relative yields of H_2CO and CH_3CHO decreased, while that of CO increased, as is show in Fig. 6. On the other hand, the distribution of the hydrocarbon products except for CH_4 was hardly affected by F in the range of 140—704 J cm^{-2}, as is shown in Fig. 7. The relative yield of C_2H_2 slightly increased, and that of Δ^1-C_4H_8 decreased, with the increase in F. Only CH_4 increased considerably with the increase in F.

The distribution of hydrocarbon products changed significantly when the laser beam was mildly focused by a 20-cm focal length lens (f), as is tabulated in Tables 5 and 6. At 0.2 J pulse^{-1}, the values of F were estimated to be 282 and 40 J cm^{-2} for lenses with 7.5- and 20-cm f respectively. In the case of a 20-cm f lens, H_2CO, C_2H_4, Δ^1-C_4H_8, and $\Delta^{1,3}$-C_4H_6 increased in their relative yields, while CO, CH_3CHO, C_3H_8, and C_3H_6 decreased and C_2H_2 was not formed, as compared to the results for 7.5-cm f. Precisely, H_2CO increased by a

Table 5. Relative Yields of Oxygen-Containing Products[a)]

f/cm	F/J cm^{-2}	Ar/Torr	Relative yield of product/%		
			CO	H_2CO	CH_3CHO
7.5	282	0	87	7	7
20	40	0	67	28	3
7.5	282	20	22	77	1

a) Yield of product relative to the total yield of oxygen-containing products. F and f denote a fluence at the focus and a focal length.

Table 6. Relative Yields of Hydrocarbon Products[a)]

f/cm	F/J cm^{-2}	Ar/Torr	Relative yield of product/%					
			C_2H_4	C_2H_2	C_3H_8	C_3H_6	Δ^1-C_4H_8	$\Delta^{1,3}$-C_4H_6
7.5	282	0	52	9	3	9	12	10
20	40	0	58	0	2	5	19	12
7.5	282	20	67	0	1	1	21	10

a) Yield of product relative to the total yield of hydrocarbon products.

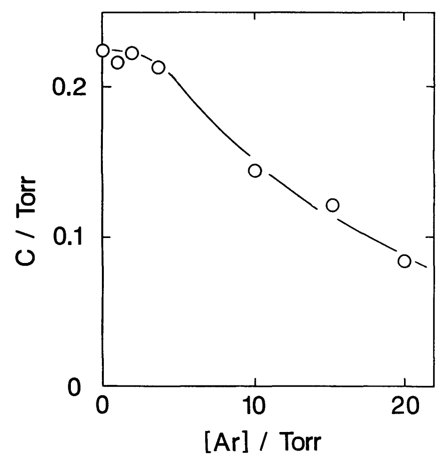

Fig. 8. Plots of C vs. Ar pressure. For experimental conditions see the captions in Figs. 1 and 2.

factor of 5, while CH_3CHO, C_3H_8, and C_3H_6 decreased to half their relative yields. The total yields of oxygen-containing products and hydrocarbon products decreased to 30 and 33% respectively. Similar resulfs were obtained for 1.0 Torr of **4**, though in this case the change in the product distribution was more significant. In the case of 20-cm f, the total product yield decreased to 23% of that for 7.5-cm f.

Under the tightly focused condition, an irradiation of less than 100 pulses produces an easily detectable amount of products. On the other hand, the products were detected by a gas chromatograph after a 1000-pulse irradiation of 3.0 Torr of **4** at 20 J cm^{-2} using the 20-cm f lens. However, no product was detected when 3.0 Torr of **4** was irradiated with 10^4 unfocused laser pulses at 0.2 J pulse^{-1} and 0.26 J cm^{-2}.

Added Gases: When 0—20 Torr of Ar was added to 3.0 Torr of **4**, the C value was measured. The addition of Ar below 4 Torr hardly affected the C value, while it

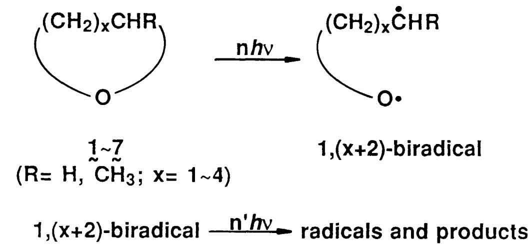

Scheme 1.

decreased significantly with an increase in the pressure of Ar over 4 Torr, as is shown in Fig. 8. The decomposition yield decreased to 37% of its initial value at 20 Torr of Ar. The addition of Ar also changed the product distribution considerably, as is tabulated in Tables 5 and 6. The relative yield of H_2CO increased, while those of CO and CH_3CHO decreased. Of the hydrocarbon products, C_2H_4 and Δ^1-C_4H_8 increased at the expense of C_2H_2, C_3H_8, and C_3H_6. The variation in the product distribution was similar to that caused by mild focusing.

Discussion

Mechanism. On the basis of the experimental results reported above, the homolytic cleavage of the C–O bond can be said to occur initially in the highly vibrationally excited ether (ether††) formed through IRMP excitation, thus yielding the corresponding biradical in Scheme 1. (The double-dagger denotes vibrational excitation). This process is similar to that in the IRMPD of open-chain ethers,[2)] in which the initial cleavage of a C–O bond yields an alkyl radical and an alkoxyl radical. The C–O bond is obviously the weakest; the dissociation energy (E_{diss}) is 74.6 kcal mol^{-1} in **3a**.[7)] The E_{diss} values have been reported to be 52, 60, and 53 kcal mol^{-1} for **1**,[11)] **2**,[12)] and **3a**[13)] respectively.

Since organic molecules are excited over the E_{diss} in the IRMPD, the primary fragments are formed with high internal energies. Therefore, the fragments decompose into stable products sequentially or through secondary IRMPD.[2,7,14] Similarly, the transient biradical intermediates are formed with high internal energies in the IRMPD of ethers, and they decompose sequentially or through secondary IRMPD. In fact, the biradical intermediates were not trapped by Br_2. This suggests that the bromine-containing compound of the biradical decomposes rapidly because an O–Br bond would be instable,[15] even if it is formed. Alternatively, it may be suggested that the transient biradical with a high internal energy decomposes, either sequentially or through secondary IRMPD within a laser pulse, before being trapped by Br_2. On the other hand, the trapping experiment of the radical species by Br_2 shows that many radical species originate from the transient biradical intermediate.

Along with Scheme 1, the mechanisms in the IRMPD of **1**—**7** under the present experimental conditions may be considered to be as follows.

1: The initial cleavage of the different C–O bonds may yield two corresponding 1,3-biradicals with high internal energies in the IRMPD of **1**. The O-radicals β-fission of the two 1,3-biradicals occurs sequentially or through secondary IRMPD. $\cdot OCH_2CH(CH_3)\cdot$ yields $H_2CO^{\dagger}$+ethylidene (CH_3CH), while $\cdot OCH(CH_3)CH_2\cdot$ yields $CH_3CHO^{\dagger}+CH_2$ or $CH_3+\cdot CH_2CHO^{\dagger}$ (Scheme 2). (The dagger denotes internal excitation). Both $H_2CO^{\dagger}$ and $CH_3CHO^{\dagger}$ decompose secondarily into H_2+CO and CH_4+CO respectively. The secondary decompositions in the relatively high yields have been discussed in the IRMPD of dimethyl and diethyl ethers in the previous study[2] and in that of **3**.[7,8] Alternatively it may be suggeted that $H_2CO^{\dagger}$ and $CH_3CHO^{\dagger}$ decompose into CO as a final oxygen-containing product through the cleavage of the C–H and C–C bonds respectively and through sequential hydrogen-abstraction from HCO by radicals, similarly to the thermolyses of H_2CO and CH_3CHO.[16]

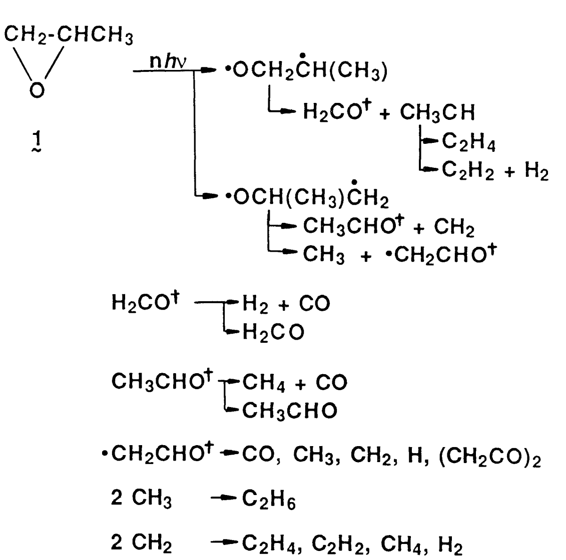

Scheme 2.

CH_3CH seems to undergo H scrambling and H_2 elimination to yield C_2H_4 and $C_2H_2+H_2$ respectively. It is well established that CH_3CH is formed as an intermediate and undergoes the same reactions in the triplet sensitized photolyses of C_2H_4.[17] The formation of C_2H_6 is explained by the radical coupling of CH_3. $\cdot CH_2CHO^{\dagger}$ decomposes into CO, CH_3, CH_2, and H or yields the low-volatile ketene dimer, since CH_2CO is not detected. CH_2 yields C_2H_4, C_2H_2, CH_4, and H_2. The formation of C_3 and C_4 hydrocarbon products in relatively lower yields can be explained by complicated pathways involving CH_2, CH_3, and the primary C_2 products.

The high yield of the secondary decomposition in the IRMPD of **1** is contrast to the relatively low yield (30—50%) in the IRMPD of dimethyl or diethyl ethers.[2] The difference is probably attributable to the high absorption energy of $\mathbf{1}^{\dagger\dagger}$ and the high strain energy of **1** (27.2 kcal mol^{-1} for propylene oxide[18]) compared with the case of open-chain ethers. Thus, the primary products are formed with relatively high internal energies in the IRMPD of **1**. Therefore, the secondary decomposition of the primary products occurs predominantly. From the yield of CO relative to the total oxygen-containing product yield in Table 2, it is generally true that the secondary decomposition of $H_2CO^{\dagger}$ and $CH_3CHO^{\dagger}$ occurs in high yields in the IRMPD of such cyclic mono-ethers as **1**, **3**, **4**, and **5** (though not for **2**). A similar mechanism involving the cleavages of the two different C–O bonds has been proposed in the thermolysis of **1**.[11] $\cdot OCH_2CH(CH_3)\cdot$ and $\cdot OCH(CH_3)CH_2\cdot$ form C_2H_5CHO and CH_3COCH_3 respectively via intramolecular H transfer in the thermolysis. On the other hand, the same biradicals are not stabilized into these compounds but decompose sequentially or through the secondary IRMPD into $H_2CO^{\dagger}+CH_3CH$ and into $CH_3CHO^{\dagger}+CH_2$ (or $CH_3+\cdot CH_2CHO$) respectively (Scheme 2). This difference can be explained by the higher internal energy contents of the biradicals in the IRMPD of **1** compared with those in the thermolysis.

2: The products in the IRMPD of **2** were CO, H_2CO, C_2H_4, and C_2H_2. The simple distribution of the products is consistent with the cleavage of the C–O bond to yield $\cdot OCH_2CH_2CH_2\cdot$. The 1,4-biradical decomposes further via radical β-fission into $H_2CO^{\dagger}$ and $C_2H_4^{\dagger}$ (Scheme 3). According to this mechanism, $H_2CO^{\dagger}$ and $C_2H_4^{\dagger}$ are formed in the ratio of 1:1. This is confirmed by the ratio of $([C_2H_4]+[C_2H_2])/([CO]+[H_2CO])=1.1$. Alternatively the concerted decomposition of $\mathbf{2}^{\dagger\dagger}$ into $H_2CO^{\dagger}$ and $C_2H_4^{\dagger}$ without the intermediary of $\cdot OCH_2CH_2CH_2\cdot$ can be suggested.

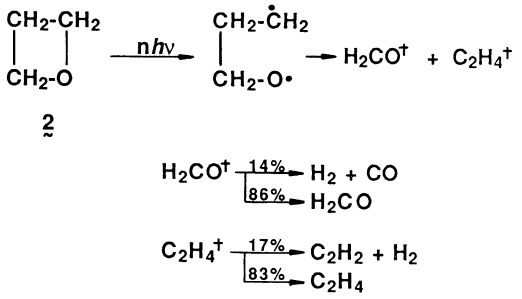

Scheme 3.

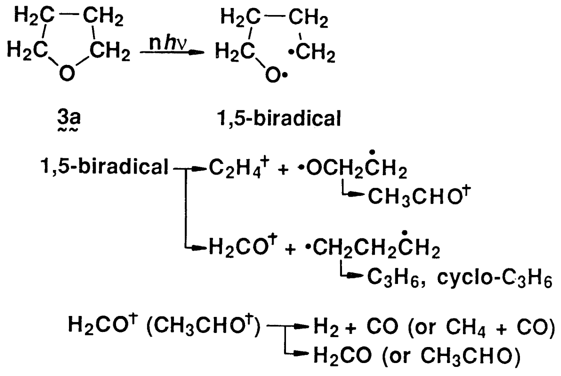

Scheme 4.

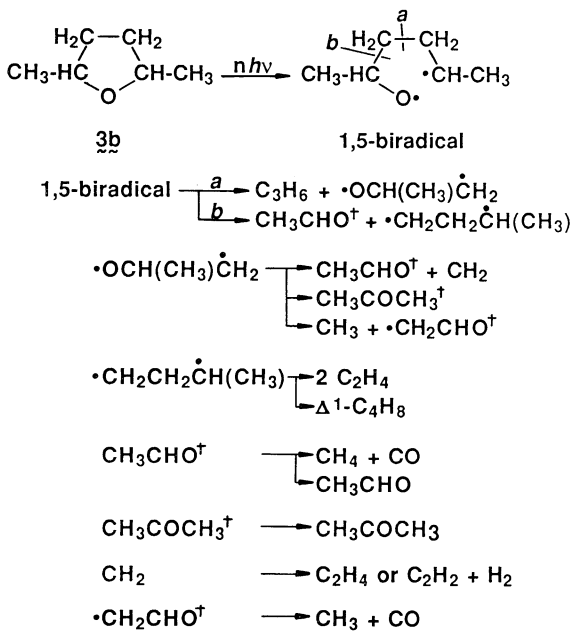

Scheme 5.

The secondary decomposition of $H_2CO^\dagger$ and $C_2H_4^\dagger$ occurs in 14 and 17% yields respectively. These yields are considerably lower than those in the IRMPD of **1**, **3**, **4**, and **5**. This may be attributable to the low E_{diss} for the concerted pathway. In the concerted process, $H_2CO^\dagger$ and $C_2H_4^\dagger$ are formed with a relatively low internal energy. Therefore, the secondary decomposition occurs in a lower yield. The concerted pathway has also been proposed in the thermolysis of **2**.[12,19] Since $\cdot OCH_2CH_2CH_2\cdot$ is formed with enough internal energy for the cleavage of the C–C bond, radical β-fission probably proceeds very rapidly. The product distribution can not distinguish clearly the concerted process from the step-by-step process via the IRMPD of the 1,4-biradical. Consequently, it is found that the structure of the cyclic ethers plays an important role in the determination of the decomposition pattern.

3a: The IRMPD of **3a**[7] and **3b**[8] has already been reported by Kramer, although the products have not been fully analyzed. We have studied the IRMPD of **3a** and **3b** in order to compare it with the IRMPD of the other ethers. Since our experimental results were essentially similar to Kramer's,[7,8] the same mechanism as in the previous studies may be proposed for the IRMPD. Following the initial cleavage of the C–O bond, $\cdot CH_2CH_2CH_2CH_2O\cdot$ further decomposes via the cleavage of two C–C bonds (Scheme 4). The $\cdot CH_2CH_2CH_2CH_2O\cdot$ splits into $C_2H_4+\cdot CH_2CH_2O\cdot$ and $H_2CO+\cdot CH_2CH_2CH_2\cdot$; the channels require 94.4 and 83.9 kcal mol^{-1} respectively as the activation energies (E_a).[7,16] Therefore, the latter splitting rather than the former is the thermodynamically favored pathway. $\cdot CH_2CH_2O\cdot$ and $\cdot CH_2CH_2CH_2\cdot$ rearrange mainly to $CH_3CHO^\dagger$ and to C_3H_6 or cyclopropane (*cyclo*-C_3H_6) respectively. In the thermolysis, $\cdot CH_2CH_2O\cdot$ yields not only CH_3CHO, but also *cyclo*-C_2H_4O. However, *cyclo*-C_2H_4O was not observed as a product in the IRMPD of **3a**. The collisional deactivation is not effective in stabilizing *cyclo*-C_2H_4O with a high internal energy under our experimental conditions. Therefore, *cyclo*-C_2H_4O is not formed, while $\cdot CH_2CH_2O\cdot$ rearranges mainly to $CH_3CHO^\dagger$ with a high internal energy and then further decomposes to $CH_4^\dagger+CO$.

3b: The initial cleavage of the C–O bond of **3b** yields $\cdot OCH(CH_3)CH_2CH_2CH(CH_3)\cdot$ with a high internal energy. The 1,5-biradical further decomposes via the cleavage of two C–C bonds, as is shown in Scheme 5. The *a* cleavage should be the main channel, because the yield of C_3H_6 is 60% of the total yield of the hydrocarbon products. The *b* cleavage, leading to the formation of CH_3CHO, is thermodynamically more favored than the *a* cleavage.

The $\cdot OCH(CH_3)CH_2\cdot$ produced in *a* cleavage isomerizes into CH_3COCH_3 via H-atom migration. At the same time, the radical may decompose into CH_2+CH_3CHO or CH_3+CH_2CHO. Further decomposition of CH_3CHO and CH_2CHO may produce CH_4+CO and CH_3+CO respectively, as has been proposed for the radical in the IRMPD of **1**. However, we could not detect CH_3COCH_3 in the IRMPD of **1**, probably because the decomposition occurred more rapidly than the H-atom migration. CH_3CHO is also produced directly from the *b* cleavage in the 1,5-biradical. The hydrocarbon biradical $\cdot CH_2CH_2CH(CH_3)\cdot$ subsequently decomposes into $2C_2H_4$ or rearranges into 1-butene (Δ^1-C_4H_8). The material balance on the basis of C-atoms was calculated to be $\{3[C_3H_6]+2([C_2H_2]+[C_2H_4]+[C_2H_6])+[CH_4]\}/(6[\mathbf{3b}])=40\%$. This relatively low value seems to suggest that a significant fraction of $\cdot CH_2CH_2CH(CH_3)\cdot$ is converted into a large molecule via a complicated reaction with some reactive species.

Kramer has reported that C_2H_6 is the second largest product at 0.3 Torr of **3b**.[8] He has pointed out that the E_a for the cleavage of the C–CH_3 bond is only 5.4—7.8 kcal mol^{-1} higher than that for the cleavage of the C–O bond in **3b**. Therefore, he has proposed that the cleavage of C(2)–CH_3 or C(5)–CH_3 bonds occurs initially. The 5-methyltetrahydrofuran-2-yl radical and CH_3 are thus formed. The former radical decomposes into fragments, while CH_3 yields C_2H_6 via coupling. However, C_2H_6 was formed in only a 4% yield relative to the total hydrocarbon yield at 3.0 Torr of **3b** (Table 2). CH_3COCH_3 was formed in a 10% yield relative to the total yield of the oxygen-containing products, although Kramer did not detect acetone. These results show that the initial cleavage of the C–O bond occurs at 3 Torr of **3b**. The high-energy channel occurs more than the low-energy channel at a lower pressure. Therefore, it is possible that the cleavage of the C–CH_3 bond partly occurs at 0.3 Torr of **3b**.

4: Following the initial cleavage of the C–O bond, $\cdot CH_2CH_2CH_2CH_2CH_2O\cdot$ further decomposes via competitive cleavages of three C–C bonds denoted by *a*, *b*, and *c* in Scheme 6. The 1,6-biradical splits into $H_2CO^\dagger+\cdot CH_2CH_2CH_2CH_2\cdot$ (Pathway *a*) and into $C_2H_4^\dagger+\cdot CH_2CH_2CH_2O\cdot$ (Pathway *b*) via radical β-fission pathways. Pathway *a* is thermodynamically favored over *b*, similarly to the cleavage of the 1,5-biradical formed in the IRMPD of **3a**. $\cdot CH_2CH_2CH_2CH_2\cdot$ and $\cdot CH_2CH_2CH_2O\cdot$ further yield $C_2H_4^\dagger$, Δ^1-C_4H_8 (or 1,3-butadiene ($\Delta^{1,3}$-C_4H_6)) and $H_2CO^\dagger+C_2H_4^\dagger$. The formation of C_3 hydrocarbons and CH_3CHO in lower yields suggests that the radical γ-fission pathway (*c*) occurs as a minor pathway. In Pathway *c*, $\cdot CH_2CH_2CH_2\cdot$ and $\cdot CH_2CH_2O\cdot$ are formed and rearrange to C_3 hydrocarbons and CH_3CHO respectively. C_4 hydrocarbons are formed only in Pathway *a*, while C_3 hydrocarbons are formed in Pathway *c*.

5: The most important feature is that 1-pentene (Δ^1-C_5H_{10}) is formed as the main product. The initial cleavage of the C–O bond yields $\cdot CH_2CH_2CH_2CH_2CH_2CH_2O\cdot$ with a high internal energy. The 1,7-biradical further splits into $H_2CO^\dagger$, $C_2H_4^\dagger$, and other biradicals via two β-fission and two γ-fission pathways (Scheme 7). $\cdot CH_2CH_2CH_2CH_2CH_2\cdot$ rearranges to Δ^1-C_5H_{10} and decomposes into $C_2H_4^\dagger+\cdot CH_2CH_2CH_2\cdot$. The rearrangement and the decomposition of the other smaller biradicals have already been discussed in connection with the IRMPD of **3** and **4**. The formation of Δ^1-C_5H_{10} as the main product suggests that the β-fission pathway to $H_2CO^\dagger+\cdot CH_2CH_2CH_2$-

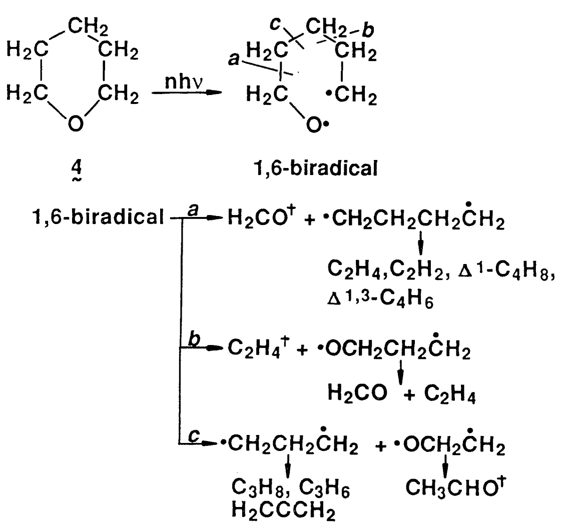

Scheme 6.

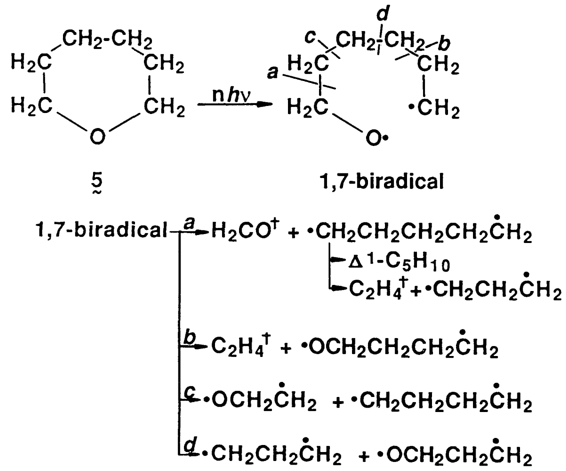

Scheme 7.

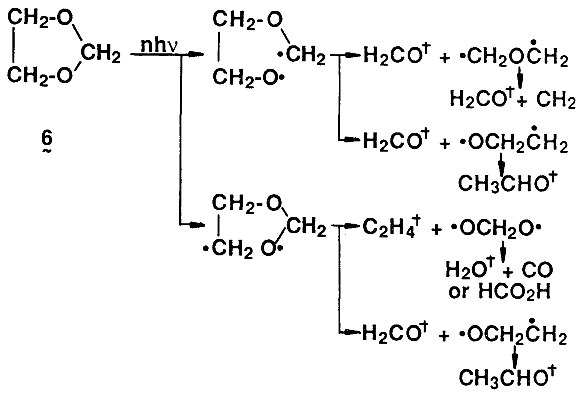

Scheme 8.

$CH_2CH_2\cdot$ is much more favored than the others.

6: In contrast to **1**—**5**, **6** and **7** have two oxygen atoms in the rings. There are two kinds of C–O bonds in **6**, with similar E_{diss} values. The initial cleavages of both C–O bonds are involved in the IRMPD of **6**, as is shown in Scheme 8, and two 1,5-biradicals are generated. $\cdot CH_2OCH_2CH_2O\cdot$ further splits into $H_2CO^{\dagger}+\cdot CH_2CH_2O\cdot$ and into $H_2CO^{\dagger}+\cdot CH_2OCH_2\cdot$, while $\cdot CH_2CH_2OCH_2O\cdot$ splits into $H_2CO^{\dagger}+\cdot CH_2CH_2O\cdot$ and into $C_2H_4^{\dagger}+\cdot OCH_2O\cdot$. The 1,3-biradical, $\cdot CH_2CH_2O\cdot$, rearranges to $CH_3CHO^{\dagger}$ or decomposes into $H_2CO^{\dagger}+CH_2$. The 1,3-biradicals $\cdot CH_2OCH_2\cdot$ and $\cdot OCH_2O\cdot$ decompose into $H_2CO^{\dagger}+CH_2$, and probably into $H_2O^{\dagger}+CO$ as well. There is a possibility that $\cdot OCH_2O\cdot$ rearranges into HCO_2H. The formation of CH_4 among the hydrocarbon products suggests that $CH_3CHO^{\dagger}$ decomposes into CH_4+CO in a high yield and that CH_2 also leads to the formation of C_2H_4 or $C_2H_2+H_2$, much as in the IRMPD of **1** and **3b**.

7: The main products in the IRMPD of **7** were CO, H_2CO, and C_2H_4. The simple distribution of the products suggests that the initial cleavage of the C–O bond is followed by the sequential formation of $H_2CO^{\dagger}$ and $C_2H_4^{\dagger}$ via radical β-fission (Scheme 9). Two β-fission pathways are involved in the secondary decomposition of the 1,6-biradical ($\cdot OCH_2CH_2OCH_2CH_2\cdot$). However, both pathways yield $H_2CO^{\dagger}$ and $C_2H_4^{\dagger}$.

Consequently, the mechanisms in the IRMPD of **1**—**7** under the present experimental conditions may be summarized as follows. The initial process in ether†† is the homolytic cleavage of the C–O bond to yield the corresponding 1, $(x+2)$-biradical with a high internal energy (Scheme 1). The biradical then further decomposes and rearranges into the primary products, mainly via radical β-fission. Since the primary products are also formed with a high internal energy, they decompose partly into the final products, either sequentially or through secondary IRMPD.

Alternatively, the concerted decomposition of ether†† into the primary products without an intermediary of a 1,4-biradical may take place in the IRMPD of **2**, considering the product distribution. In the IRMPD of **6** and **7**, the simple product distributions suggest that the concerted decomposition into the primary products occurs competitively with the biradical mechanism. When the sequential decomposition of the biradical intermediates occurs rapidly, the product distribution is rather simple and similar to that in the concerted pathway. Therefore, we can not recognize a clear difference between the two mechanisms with respect to the product distribution.

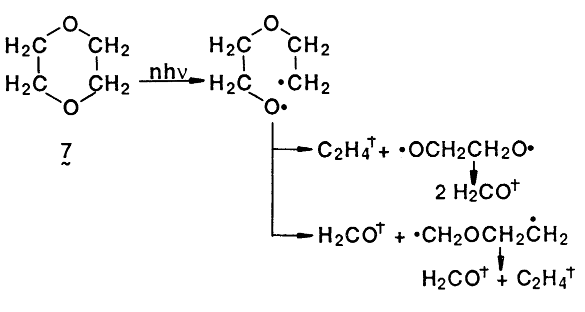

Scheme 9.

Effects of Irradiation Parameters in the IRMPD of 4. We have estimated the branching ratios of several competitive pathways in the primary and secondary cleavages on the basis of the product distribution. However, the product distribution depends on the irradiation parameters in the IRMPD of organic compounds.[1,4,5,14,20,21] In fact, we have found that the distribution of the products varies with the laser fluence, the pressure, and the additive gases in the IRMPD of **4**.

As is shown in Fig. 5, C increased with an increase in F according to the relation of $C \propto F^{1.7}$. Assuming a 3/2 power law in a focused beam geometry,[22] the value of $k_d=8.5\times10^{-4}$ pulse^{-1} leads to a threshold fluence of 5.2 J cm^{-2}.

Branching Ratio of Sequential Decomposition: The predominant formation of C_2 bromine-containing compounds indicates that Pathways a and b occur mainly in the IRMPD. In addition, the formation of C_4 and C_3 bromine-containing compounds clearly shows the participation of Pathways a and c respectively. However, the considerable amounts of C_1 bromine-containing products suggest that some pathways to yield C_1 fragments are involved in the sequential decomposition of the transient biradicals, radicals, and primary products.

Accroding to Scheme 6, H_2CO and C_2H_4 are the main products from Pathways a and b, while C_4 hydrocarbons are formed only in Pathway a. The products in Pathway c are mainly C_3 hydrocarbons and CH_3CHO. Therefore, the branching ratio of Pathway c can easily be estimated to be 0.18 from [C_3 hydrocarbons]/(0.5×[C_2 hydrocarbons]+[C_3 hydrocarbons]+[C_4 hydrocarbons]). The relatively small ratio of 0.18 for 3.0 Torr of **4** at 282.2 J cm^{-2} can be explained by the higher energy required for Pathway c than for a or b.

The decomposition yield increased with an increase in the number of pulses, according to the first-order kinetics. The product distribution is almost invariant if the number of pulses is less than 600 with a conversion of 40%. These results suggest that unimolecular decomposition occurs at a constant branching ratio among the competitive pathways in Scheme 6. However, the decomposition yield and the product distribution were apparently changed by variations in other irradiation parameters, such as the pressures of **4** and Ar, F, and f.

Collisional Effects: The relations of $Y \propto (P_0)^2$ in Fig. 4 and $C \propto (P_0)^2$ were obtained in the range of

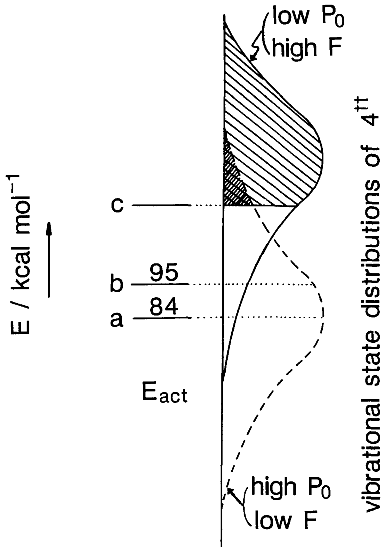

Fig. 9. Schematic diagram of the vibrational state distributions of $4^{\dagger\dagger}$ depending upon P_0 and F and activation energies (E_{act}) of Pathways a, b, and c. Shaded parts indicate the states with higher energies than E_{act} for Pathway c.

P_0=0.1—10 Torr. These results suggest that collisional up-pumping contributes to the accumulation of sufficient energy for the cleavage of the C–O bond at higher pressures of **4**.

The product distributions were significantly changed with P_0, as is shown in Figs. 3 and 4. The results are explained by collisional deactivation processes competing with the IRMP excitation and with the sequential decomposition of the transient species and the primary products. Since the rate of collisional deactivation increases with an increase in P_0, the average internal energy of $\mathbf{4}^{\dagger\dagger}$ decreases and the sequential decompositions are quenched at higher pressures, as is shown in Fig. 9. Consequently, the branching ratio of the low-energy pathway, a or b, increases, accompained with the decrease in Pathway c. The sequential decomposition of the primary products with high internal energies also decreases. In fact, the relative yields of C_2 and C_4 hydrocarbons and H_2CO in Pathways a and b increased with the increase in P_0, while those of C_3 hydrocarbons and CH_3CHO in Pathway c decreased. It was also observed that the yield of CO from the sequential decomposition of $H_2CO^{\dagger}$ and $CH_3CHO^{\dagger}$ decreased. The branching ratio of Pathway c decreased from 46 to 9% when P_0 was increased from 0.5 to 10 Torr.

It is noteworthy that the distribution of hydrocarbon products is almost independent of the P_0 value over 4 Torr. This fact suggests that not only collisional deactivation, but also other reactions between the transient radicals and **4**, occur in the IRMPD of **4**. At higher pressures, transient radicals such as 1,6-biradical, 1,4-biradicals (Scheme 6), alkyl radicals, and vinyl radicals can abstract hydrogen atoms on 2-, 3-, and 4-positions of **4** to yield 2-, 3-, and 4-tetrahydropyranyl radicals respectively. These radicals rearrange and split sequentially via the radical β-fission of C–O or C–C bonds. Thus, the decomposition should produce H_2CO and C_2 and C_4 hydrocarbons, similarly to Pathways a and b. In support of this pathway, H_2CO, C_2 and C_4 hydrocarbons were the main products at higher **4** pressures, as is shown in Figs. 3 and 4, and Y increased with the increase in P_0 with the relation of $Y \propto (P_0)^2$.

The effects of Ar on C, Y, and the product distribution suggest that collisional up-pumping and/or rotational hole-filling, as well as collisional deactivation,[23] are involved in the formation of $\mathbf{4}^{\dagger\dagger}$. These collisional processes increase with the increase in the pressures of **4** and Ar. Collisional up-pumping and rotational hole-filling lead to a higher average vibration energy of $\mathbf{4}^{\dagger\dagger}$ and higher internal energies of the primary products. On the other hand, collisional deactivation behaves in the opposite manner. Collisional up-pumping and rotational hole-filling are quantitatively comparable to collisional deactivation below 4 Torr of Ar, while collisional deactivation occurs dominantly over 4 Torr of Ar, as is shown in Fig. 8.

Internal Energy of Transient Species: The effect of F on the product distribution in Figs. 6 and 7 can be explained by the change in the sequential decomposition rate of $H_2CO^{\dagger}$ or $CH_3CHO^{\dagger}$. The increase in F enhances the rate of IRMP absorption.[21] Consequently, a larger vibrational energy is accumulated in $\mathbf{4}^{\dagger\dagger}$ and the primary products are formed with higher internal energies, as is shown in Fig. 9. Thus, the sequential decomposition of the primary products is accelerated. However, the branching ratio among the three pathways in Scheme 6 and the rates of the sequential decomposition of hydrocarbon products seem to be scarcely affected by the variation in F in 140—704 J cm^{-2}.

The effect of f on IRMPD has been well characterized using many compounds. In the IRMPD of SF_6,[24] the decomposition rate per unit of volume is independent of f at F values larger than the threshold fluence. On the other hand, the decomposition yields an increase at a shorter f in the IRMPD of *trans*-2-deuteriovinyl chloride,[25] H_2CO,[26] and tetrahydrofuran,[7] in spite of the decreasing reaction volume. The effect of f on the IRMPD of **4** in Tables 5 and 6 is similar to the latter.

It is noteworthy that the relative yields of C_4 hydrocarbons increased slightly when f was changed from 20 to 7.5 cm. The addition of Ar led to similar changes in the yields of C_4 hydrocarbons. These results are consistent with the fact that a lower energy is required for Pathway a than for b.

Comparison. In conventional pyrolyses of the cyclic ethers, a concerted decomposition occurs, together with the homolytic cleavage of a C–O bond.[11–13,27] Exceptionally, the thermolysis of **2** proceeds via only a concerted pathway, in which radical species are not involved.[12] The thermal decomposition of *cyclo*-C_2H_4O and **3a** has been studied behind reflected shocks in a single-pulse shock tube over the range of 800—1500 K.[28] The product distributions are explained mainly by concerted pathways.

On the other hand, the homolytic cleavage of a C–O bond has been considered to be a predominant pathway in the UV photolyses of cyclic ethers.[27,29] However, many competitive pathways are involved in the sequential decomposition of the biradical intermediates. Therefore, the product distributions are rather complex and are strongly dependent on the excitation procedure: the wavelength of light, direct or sensitized excitation, the light intensity, and the sample pressure.[29]

The IRMPD is essentially similar to thermolysis, although it occurs via a highly vibrationally excited molecule. The mechanism in the IRMPD of **1**—**7**, probably except for **2**, is explained by a C–O bond cleavage instead of a concerted pathway. On the other hand, the concerted pathway is consistent with the results in the shock tube pyrolyses as well as those in the conventional pyrolyses. We assume that the difference is the result of the relatively high pressures (80—400 Torr) in the pyrolyses[27,28] compared with that (3 Torr) used in the present work. At a higher pressure, the collisional deactivation must occur rapidly; therefore, the decomposition proceeds via the lowest energy channel, i.e., the concerted pathway. The product distributions in the pyrolyses are different from those in the IRMPD because of reactions between the radical species. In addition, the starting ether is easily involved in radical reactions in the pyrolyses at higher pressures. On the other hand, the ether is excited to a higher state than the lowest threshold at lower pressures in the IRMPD. Therefore, the high-energy channel occurs easily in the IRMPD. It is also noteworthy that the temperature around a focused point is estimated to be higher than 2000 K on the basis of absorbed energy per molecule. This is also consistent with the occurrence of the high-energy channel in the IRMPD.

Possibility of Oxygen-Isotope Separation. Similarly to open-chain ethers, cyclic ethers can be used as starting molecules in the oxygen-isotope separation by the use of a TEA CO_2 laser. However, the complicated decomposition pathways of biradical intermediates yield several oxygen-containing products. With respect to this point, open-chain ethers are better than cyclic ethers. The best starting ether should have a large isotope shift of absorption in the tunable range of a TEA CO_2 laser and a high selectivity of the oxygen-isotope in the C–O bond cleavage. Consequently, the best is **4** because of its high yield, simple pathway, and simple oxygen-containing product. Therefore, the ^{18}O enrichment using the IRMPD of **4** has been investigated and published separately.[30]

We wish to thank Mr. Masahiro Toyoda, undergraduate student of Science University of Tokyo in 1982—1983, for his help in a part on the experiments.

References

1) Part III: T. Majima and T. Ishii, *Nippon Kagaku Kaishi*, **1989**, 1225.

2) T. Majima, T. Ishii, and S. Arai, *Bull. Chem. Soc. Jpn.*, **62**, 1701 (1989).

3) V. V. Vizhin, Y. N. Molin, A. K. Petrov, and A. R. Sorokin, *Appl. Phys.*, **17**, 385 (1978).

4) K. O. Kutschke, C. Willis, and P. A. Hackett, *J. Photochem.*, **21**, 207 (1983).

5) T. Majima, T. Igarashi, and S. Arai, *Nippon Kagaku Kaishi*, **1984**, 1490.

6) D. M. Brenner, *J. Phys. Chem.*, **86**, 41 (1982).

7) J. Kramer, *J. Phys. Chem.*, **86**, 26 (1982).

8) J. Kramer, *J. Photochem.*, **24**, 11 (1984).

9) W. E. Farneth and D. G. Johnson, *J. Am. Chem. Soc.*, **106**, 1875 (1984).

10) S. Ruhman, O. Anner, S. Gershuni, and Y. Haas, *Chem. Phys. Lett.*, **99**, 281 (1983); S. Ruhman, O. Anner, and Y. Haas, *J. Phys. Chem.*, **88**, 5162 (1984); Y. Haas, S. Ruhman, G. D. Greeblatt, and O. Anner, *J. Am. Chem. Soc.*, **107**, 5068 (1985).

11) T. J. Hardwick, *Can. J. Chem.*, **46**, 2453 (1968); A. T. Blades, *ibid.*, **46**, 3283 (1986).

12) D. A. Bittker and W. D. Walters, *J. Am. Chem. Soc.*, **77**, 1429 (1955).

13) W. B. Guenther and W. D. Walters, *J. Am. Chem. Soc.*, **73**, 2127 (1951).

14) W. E. Farneth and M. W. Thomsen, *J. Am. Chem. Soc.*, **105**, 1843 (1983).

15) R. T. Sanderson, "Chemical Bonds and Bond Energy," 2nd ed, Academic Press, New York (1976).

16) S. W. Benson, "Thermochemical Kinetics," 2nd ed, Wiley, New York (1976).

17) R. J. Cvetanovic and A. B. Callear, *J. Chem. Phys.*, **23**, 1182 (1955); A. B. Callear and R. J. Cvetanovic, *ibid.*, **24**, 873 (1956).

18) K. Pihlaja and E. Taskinen, "Physical Methods in Hetero-cyclic Chemistry," ed by A. B. Katritzky, Academic Press, New York (1974), Vol. 6, p. 199.

19) K. A. Holbrock and R. A. Scott, *J. Chem. Soc., Faraday Trans. 1*, **71**, 1849 (1974).

20) V. S. Letokhov, "Non-linear Laser Chemistry," Springer-Verlag, Berlin (1983).

21) W. C. Danen and J. C. Jang, "Laser-Induced Chemical Processes," ed by J. I. Steinfeld, Plenum Press, New York (1981), p. 45.

22) S. Speiser and J. Jortner, *Chem. Phys. Lett.*, **44**, 399 (1976).

23) P. A. Hackett, C. Willis, and M. Gauthier *J. Chem.*

Phys., **71**, 2682 (1979); M. Gauthier, P. A. Hackett, and C. Willis, *Chem. Phys.*, **45**, 39 (1980).
24) P. Fettwewis and M. Meve de Mevergnies, *Appl. Phys.*, **12**, 219 (1977).
25) C. Reiser, F. M. Lussier, C. C. Jenses, and J. I. Steinfeld, *J. Am. Chem. Soc.*, **101**, 350 (1979).
26) G. Koren, *Appl. Phys.*, **21**, 65 (1980).
27) S. Braslausky and J. Heicklen, *Chem. Rev.*, **77**, 473 (1977).
28) A. Lifshitz and H. Ben-Hamou, *J. Phys. Chem.*, **87**, 1782 (1983); A. Lifshitz, M. Bidani, and S. Bidani, *ibid.*, **90**, 3422 (1986).
29) C. Sonntag and H.-P. Schuchmann, *Adv. Photochem.*, **10**, 59 (1979).
30) T. Majima, K. Sugita, and S. Arai, *Chem. Phys. Lett.*, **163**, 29 (1989).